HHS Public Access

Author manuscript

*Magn Reson Med*. Author manuscript; available in PMC 2017 May 01.

Published in final edited form as:

*Magn Reson Med*. 2016 May ; 75(5): 1978–1988. doi:10.1002/mrm.25797.

# Fat-suppressed Alternating-SSFP for Whole-Brain fMRI using Breath-hold and Visual Stimulus Paradigms

**Tiffany Jou**[1], **Steve Patterson**[2], **John M. Pauly**[1], and **Chris V. Bowen**[3]

[1]Magnetic Resonance Systems Research Laboratory, Department of Electrical Engineering, Stanford University, Stanford, California

[2]Biomedical Translational Imaging Centre, Halifax, Nova Scotia, Canada

[3]Department of Radiology, Dalhousie University, Halifax, Nova Scotia, Canada

## Abstract

**Purpose—**To achieve artifact-suppressed whole-brain pass-band balanced SSFP (pb-SSFP) functional MRI from a single fMRI scan.

**Methods—**A complete and practical data acquisition sequence for alt-SSFP fMRI was developed. First, multi-shot flyback-EPI and echo-time shifting were used to achieve data acquisition that was robust against eddy currents, gradient delays, and ghosting artifacts. Second, a steady-state catalyzation scheme was implemented to reduce oscillations in the transient signal when catalyzing in and out of alternate steady states. Next, a short spatial-spectral RF pulse was designed to achieve excellent fat-suppression while maintaining a repetition time < 15 ms to sensitize functional activation toward smaller vessels and capillaries. Lastly, parallel imaging was used to achieve whole-brain coverage and sufficiently high temporal resolution.

**Results—**Breath-hold experiments showed excellent fat-suppression and alt-SSFP's capability to recover functional sensitivity from signal dropout regions of conventional GRE and banding artifacts from conventional pb-SSFP. Applying fat-suppression resulted in improved activation maps and increased temporal SNR. Visual stimulus functional studies verify the proposed method's excellent functional sensitivity to neuronal activation.

**Conclusion—**Artifact-suppressed images are demonstrated, showing a practical pb-SSFP fMRI method that permits whole-brain imaging with excellent BOLD sensitivity and fat suppression.

### Keywords

balanced-SSFP; BOLD; fMRI; whole-brain; alternating-SSFP; fat-suppression

## Introduction

The most widely used methods to acquire functional magnetic resonance imaging (fMRI) images are $T_2$*-weighted Gradient-Echo (GRE) sequences, which exhibit excellent

*Address correspondence to:* Tiffany Jou, Packard Electrical Engineering, Room 208, 350 Serra Mall, Stanford, CA 94305-9510, TEL: (619) 855-5267, tjou@stanford.edu.

sensitivity to Blood Oxygen Level Dependent (BOLD) contrast (1). However, GRE sequences require a long echo time (TE) for BOLD sensitivity and use long, single-shot readouts for efficiency, resulting in artifacts such as signal dropout and image distortion in regions with severe magnetic field inhomogeneity near air-tissue interfaces, such as the temporal lobe and orbitofrontal cortex. Many groups have been investigating alternatives to GRE sequences for fMRI to mitigate these artifacts, such as using spin-echo and other $T_2$-weighted sequences. Spin-echo methods refocus static field inhomogeneities, recovering signal dropout regions (2). Unfortunately, these methods suffer from a significant loss in functional BOLD sensitivity (3). The Small-tip Fast Recovery (STFR) sequence is a recently proposed method that has been shown to produce functional contrast at short TE (4). This is a promising alternative to long-TE GRE sequences, but the implementation currently requires a subject-specific design of tailored RF pulses calculated from accurately acquired $B_0$ field maps.

Several studies have shown promising results with fMRI acquisition methods based on balanced steady-state free precession (bSSFP) including transition-band balanced-SSFP (tb-SSFP) (5–7) and pass-band balanced-SSFP (pb-SSFP) (8–11). Compared to transition-band balanced-SSFP, pass-band balanced-SSFP is less sensitive to off-resonance frequency shifts and requires fewer phase-offset acquisitions to achieve reliable BOLD contrast with whole-brain coverage.

Depending on the applied TR and flip angle, the contrast mechanism of pb-SSFP for BOLD fMRI consists of a combination of $T_2$ contrast, including diffusion sensitivity to microscopic field inhomogeneities surrounding micro-vasculature, and $T_2$* contrast. At short TR, the source of contrast has been shown to be mainly from intravascular $T_2$ change and diffusion of extravascular spins (12,13). Therefore, pb-SSFP has several advantages over conventional GRE-EPI acquisitions, including small-vessel BOLD sensitivity, reduced image distortion, and reduced signal dropout from susceptibility field gradients due to the short TE and rapid acquisition (11).

Despite these advantages, pb-SSFP methods exhibit off-resonance banding artifacts that must be addressed for robust whole brain fMRI. There are several different methods that address this issue. For a limited ROI, these bands can be avoided altogether through careful shimming. For whole-brain acquisitions, shimming is insufficient to eliminate all banding and one approach is the two-acquisition method (10). This approach removes banding artifacts by combining images from two acquisitions having different RF phase-cycling in repeated fMRI scans to spatially shift bands that can be eliminated in post-processing through maximum intensity projection (MIP) image combination. The entire fMRI paradigm is repeated (once for each RF phase-cycled acquisition) to allow sufficient time for steady state to be re-established following a change in the RF phase-cycling increment. However, for most neuroscientific applications, repeating the entire fMRI paradigm produces confounding effects from cognitive habituation to stimuli and is not ideal.

This paper describes the development of an improved balanced-SSFP fMRI technique called alternating-SSFP (alt-SSFP) which permits whole-brain, banding-artifact-free balanced-SSFP fMRI in a single fMRI scan. Alt-SSFP uses RF catalyzation, a short sequence of

preparatory RF pulses applied prior to data acquisition and designed to expedite the establishment of steady-state, to enable quick alternation between two RF phase-cycling steady states to acquire a single functional volume. This approach requires high flip angles (>30°) and short TR (<15 ms) for optimal acquisitions. The feasibility of this method has been previously demonstrated through Monte Carlo simulations and preliminary studies (14). However, issues involving fat signal suppression and image acceleration were not addressed in these studies and are required for practical implementation in whole-brain fMRI applications.

Balanced SSFP sequences characteristically result in bright signal for tissues having large $T_2/T_1$ ratios such as fat (15). Fat signal is particularly problematic for EPI trajectories, since k-space is traversed relatively slower in the phase-encode direction, producing significant chemical-shift artifact that overlaps cranial fat with cortical regions. Chemical-shift artifacts cause skull-stripping and brain extraction tools to perform poorly. This results in poor intra-subject alignment between the low-resolution functional images and high-resolution anatomical images which reduces the accuracy and reliability of fMRI analysis. In addition, off-resonance fat signal is also more susceptible to signal fluctuations following RF catalyzation and can result in increased phase encode ghosts (16).

Spatial-spectral pulses (SPSP) are used to excite magnetization that is both spatially and spectrally selective and are effective in fat suppression by not exciting fat signal at all (17–19). This is a simple and straightforward way to apply fat suppression in the alt-SSFP fMRI sequence. However, SPSP RF pulses are relatively long-duration pulses, so special considerations are required (20). Increasing the minimum TR of the sequence would not only introduce more banding artifacts, but could also increase the TR beyond the desired limit for optimal BOLD contrast. Optimal implementation of bSSFP sequences for fMRI applications requires that TR be less than 15 ms in order to maximize functional sensitivity to diffusion around capillaries of radius 2 μm – 5 μm (11), and also that volume TR be 3 s or less. Shortening an SPSP pulse would either reduce the stop band null bandwidth, increasing the sensitivity to $B_0$ variation, or the frequency of fat would simply reside within the widened spectral pass-band. On the other hand, it is important to maintain a sharp spatial excitation profile due to the sensitivity of the SSFP off-resonance profile to flip angle (21). Therefore, a design for a short duration spatial-spectral pulse effective enough to be both spectrally and spatially selective within this short TR range is needed for alt-SSFP implementation.

In this study, we propose a fat-suppressed alt-SSFP method as the first practical implementation of pass-band balanced SSFP for fMRI and demonstrate good BOLD sensitivity in both breath-hold and visual stimulus paradigms. We have integrated parallel imaging into the alt-SSFP sequence to increase spatial resolution and volumetric coverage for whole brain applications. We have specifically designed a short-duration spatial-spectral (SPSP) pulse that suppresses bright fat signal. Using human breath-holding experiments, the objectives of our study were to show that by using only a single fMRI scan, alt-SSFP recovers functional sensitivity in regions that suffer 1) signal dropout in GRE-EPI, and 2) banding artifacts in conventional pb-SSFP. In addition, including our designed short spatial-spectral pulse suppresses bright fat-shift artifacts while increasing overall temporal SNR.

Finally, we demonstrate the functional sensitivity of fat-suppressed alt-SSFP to neuronal activation using a visual stimulation paradigm in human subjects.

## Methods

Alt-SSFP enables single-scan fMRI studies by alternating between two phase-cycled steady states (180° and 0°) throughout the fMRI scan. This approach requires high flip angles (> 30°) and short TR (< 15 ms) for optimal acquisitions, and ideally a total volume time $T_{vol}$ (defined as total time to acquire a 180°, 0° phase-cycled image volume pair) of 3 s or less to have good statistical power, temporal resolution, and functional contrast. Therefore, each phase-cycled steady state volume is to be acquired in half the total volume time. In addition, to alternate between steady states, catalyzation methods should be used to ensure signal stability.

The following sections will discuss issues addressed in pulse sequence development.

### Data Acquisition

A 3D multi-shot fly-back EPI sequence with an echo train length of 4 was used, as shown in Fig 1. Flyback EPI was used for robustness against eddy currents and gradient delay (22). In interleaved multi-shot EPI, each group of echoes during a certain shot is modulated by the phase associated with its readout time. This results in a staircase phase modulation, which leads to ghosting in the phase-encoding direction. Echo-time shifting was used to mitigate this ghosting caused by phase accrual. (23,24).

BOLD contrast in alt-SSFP is suppressed immediately following the catalyzation RF pulse train and increases during the data acquisition train (14). Therefore, the center of k-space was acquired near the end of each 3D volume to ensure sufficient BOLD contrast had developed and to ensure signal stability when center of k-space had been reached. Data acquisition order consisted of $k_z$ encodes in the outer loop and $k_y$ views in the inner loop. $k_z$-Phase-encodes were acquired in reverse-centric order, as shown in Fig 1(c).

### Catalyzation to Steady-state

In alt-SSFP, image volumes are acquired during 0° and 180° RF phase-cycled steady states in an interleaved fashion, instead of staying in one steady-state for the entire fMRI scan. Imaging during the transient response produces signal fluctuation phase-encode artifacts, but the transient response can be catalyzed into the steady state by manipulating RF pulses, in order to not have to wait until oscillations decay (25).

Several methods have been proposed to reduce these transient oscillations, including $\alpha/2$ preparation (26), catalyzation (25), variable flip-angle method (27), Kaiser Bessel windowed ramp method (28), and linear flip method (16). Alt-SSFP uses the linear flip method, where the flip angles linearly increase during the dummy cycles before acquisition. This method is relatively simple and has been shown to result in better stability across all resonance frequencies (16) compared to the $\alpha/2$ preparation method. Ten dummy cycles were used for RF linear flip-angle catalyzation to transition to the next (0° or 180°) RF phase-cycling steady state. A $90° - \alpha/2$ flip-down pulse (14) is applied at the end of a 3D image volume to

put magnetization into the transverse plane to be spoiled. A gradient spoiler after the flip-down pulse was implemented to null what is left in the transverse plane before linear catalyzing into the next phase-cycled steady state. This greatly reduces the signal oscillations in alt-SSFP since pass-band signal from one acquisition becomes stop-band signal in the next acquisition and is vulnerable to oscillation during catalyzation. The alternating-SSFP catalyzation scheme is depicted in Fig 2.

### Fat Signal Suppression

A short true-null SPSP RF pulse with nominal duration of 4.35 ms was designed (17). For the spectral profile, a TBW = 2 Dolph-Chebyshev window was used for the main envelope with 40 dB stop-band ripples (29). The Chebyshev window exhibits a tighter spectral transition-band compared to methods such as a sinc or Hann window. The tighter transition-band of this filter widens the stop-band null bandwidth, which decreases the sequence's sensitivity to $B_0$ variation. For the spatial profile, 7 sub-pulses each with TBW = 8 and duration of 540 μs were used. Sub-pulse duration was determined by approximately placing the spectral null at the frequency of fat at 3T (−440Hz). Sub-pulses were designed to be minimum-phase to ensure optimal slice profile (29). Gradient waveforms are slew-rate limited, resulting in an RF excitation pulse of 5 ms. The RF pulse profile and corresponding gradient waveforms are shown in Fig 3(a). Simulated spectral and spatial profiles are shown in Fig 3(b) and (c).

### Acceleration

Each 3D volume was four-fold uniformly undersampled in the $k_y$ phase-encode direction to achieve whole-brain coverage and an equivalent volume time of 3.46 s. In other words, the total time needed to acquire a 180° phase-cycled or a 0° phase-cycled volume was 1.73 s. Data were reconstructed using GRAPPA (30). A fully-sampled 3D reference volume was acquired at the beginning of an fMRI scan and GRAPPA weights were calculated from the center auto-calibration region. These weights were then used for the reconstruction of the entire fMRI scan.

### Functional MRI Experiments

All experiments were performed on a GE Discovery MR750 3T system (50 mT/m maximum gradient strength and 200 mT/m/ms maximum slew rate) with a 32-channel head coil (Nova Medical Inc.). A total of 11 normal and healthy volunteers participated in the study with the approval of the Stanford University Institutional Review Board (6 males, 5 females). All subjects were individually recruited for breath-hold and visual studies; some subjects participated in both studies in separate sessions.

Alt-SSFP experiments were conducted with the following parameters: TR = 14.3 ms, flip angle = 35°, acquisition matrix = 80 × 80 × 22, receiver bandwidth = ±62.5 kHz. Two dummy scans were acquired in the beginning of each scan, in addition to one fully-sampled reference scan used for GRAPPA reconstruction. For comparison, a 2D single-shot EPI GRE sequence was performed with a flip angle = 77°, and TE = 30 ms. The TR of the GRE sequence was prescribed as the total time to acquire all the 2D slices, which was made equal to the total volume time of the 3D alt-SSFP sequence (3.46 s). GRE-EPI and alt-SSFP fMRI

experiments were conducted with identical spatial and temporal resolution for each type of stimulus study. A high resolution $T_1$-weighted anatomical scan was obtained after each set of fMRI scans for co-registration and group-analysis purposes.

### Breath-holding Experiment

Breath-holding, which induces hypercapnia, was used to elicit whole-brain activation. This induced hypercapnia increases oxygenation across the entire brain by increasing cerebral blood flow (31). These experiments were done to demonstrate the capability of alt-SSFP to exhibit artifact-suppressed whole-brain activation. Data were acquired at a spatial resolution of $3 \times 3 \times 5$ $mm^3$ with an FOV = $24 \times 24 \times 11$ $cm^3$. Subjects performed 6 alternating blocks of 20.8 s self-paced breathing and breath-holding on expiration for each run for a total of 5 min. Trial timing was cued by PsychoPy (32). Respiratory bellows were used to monitor the breathing pattern of the subject. The self-paced breathing block included a rest phase and preparation phase where the final two inhale-exhale cycles before breath-hold were cued visually to reduce variation across subjects. The breath-holding block was cued by a circle that decreased in size during breath holding and disappeared at the end of the block.

### Visual Stimulus Experiment

A simple visual stimulus study was used to demonstrate functional sensitivity of alt-SSFP to actual neuronal activation. The data were acquired at a spatial resolution of $3 \times 3 \times 3$ $mm^3$ with an FOV = $24 \times 24 \times 6.6$ $cm^3$ covering the visual cortex region. Visual stimulus experiments were performed using 6 alternating blocks of 20.8 s each of left versus right visual field stimulation for a total of 5 min.

### Data Analysis

Maximum Intensity Projection (MIP) was used to combine each 180°, 0° phase-cycling volume pair. The mean functional images from the entire fMRI run were used to compute the MIP pixel selection mask so that each pixel was selected from one phase-cycling angle image throughout the time series (10). Another method for computing the MIP mask would be to compute pair-wise MIP masks for each phase-cycled volume pair. The prior MIP method (mean MIP mask) was chosen to be consistent with two-acquisition pb-SSFP fMRI (10). FSL (33) was used for fMRI data statistical analysis using a high-pass filter cuto of 41 s and MCFLIRT motion correction (34). Activation was modeled as a boxcar function (representing the functional paradigm) convolved with a Gaussian function. Z-scores were calculated using a cluster-level correction for multiple comparisons ($z > 2.3$, $P < 0.05$). Group statistics for the visual stimulus experiments were computed using Fixed effects (FE) higher-level modeling in FSL (33) over N = 9 subjects.

Temporal SNR (tSNR) was compared between non fat-suppressed and fat-suppressed alt-SSFP fMRI scans. tSNR maps were generated by dividing the mean signal level by the standard deviation of the GLM residuals. Mean tSNR was calculated in a gray matter ROI for each subject using FAST segmentation (35) to generate the gray matter mask. Without fat-suppression, fat shifts into the visual cortex region. With our prescribed receive bandwidth of ±62.5kHz and matrix size of $80 \times 80$, the fat-shift in the readout (A/P) direction is negligible (0.9 mm). However, for the slow $k_y$ phase-encode (L/R) direction, the

expected water-fat shift is 9.7 mm, which exceeds a 3 voxel shift. Mean tSNR was also calculated in a visual cortex ROI for N = 8 subjects for comparison between non fat-suppressed and fat-suppressed runs. Functional images were registered and warped to the MNI-152 standard brain space. Mean tSNR was computed within the V1 region of the visual cortex for each subject using the Jülich histological atlas (36) in FSL to define the mask for the region of interest.

## Results

Fig 4 shows the phase-cycled images and MIP results of a representative subject. Additional bands across the $k_y$ phase-encode direction were artificially introduced with y-shim offsets to examine the capability of alt-SSFP to reduce banding artifacts. The 180° RF phase-cycled and 0° RF phase-cycled images were produced by processing only one phase-cycling phase of the alt-SSFP images. Single phase-cycled images exhibit dark bands with very low signal and loss of functional sensitivity. After a Maximum Intensity Projection (MIP) combination of the phase-cycled image volume pairs, stop-band signal is recovered, while functional sensitivity and z-score is relatively uniform across off-resonance frequencies. Results from either a time-series mean MIP mask or a pair-wise MIP mask method showed little difference in the study, as shown in Fig 4. The proposed alt-SSFP implementation suppresses banding artifacts that would be present in bSSFP images. The absence of phase encode ghosting in the images (signal-to-ghost ratio < 5%) demonstrate that the catalyzation scheme suppresses oscillations and keeps the signal stable while transitioning between the two steady states.

Fig 5 shows results comparing non fat-suppressed and fat-suppressed alt-SSFP images with the same TR and temporal/spatial resolution. Without applying the designed SPSP RF pulse, the result is impractical as the fat signal is very bright and shifts into the brain region. Fig 5(a) shows that with the presence of bright fat shift it is difficult to apply tools for accurate brain extraction of non fat-suppressed raw images. Fig 5(b) shows poorer activation maps with lower z-scores for non fat-suppressed images. With the use of the SPSP RF pulse, the bright fat signal is greatly suppressed and functional activation is better localized in the brain region with more homogeneous functional maps.

An increase in temporal signal stability was observed in fat-suppressed images. Fig 6(a) shows select slices from a breath-hold study where tSNR was improved in regions suffering from fat-shift artifacts and overall after applying fat-suppression with the short SPSP RF pulse. Fig 6(b) and (c) show the comparison of tSNR values between non fat-suppressed and fat-suppressed scans over a group of N = 8 subjects. There was a 17% ± 4% increase in mean tSNR in fat-suppressed scans over non fat-suppressed scans in gray matter ROI during visual stimulus scans. There was a 20% ± 8% mean tSNR increase in the V1 region of the visual cortex when fat suppression was applied compared to no fat-suppression.

Alt-SSFP recovers raw signal and functional sensitivity in signal dropout regions of conventional GRE acquisitions, as shown in a representative subject in Fig 7. In GRE-EPI images (Fig 7, bottom), there exist distinct signal dropout regions in the temporal lobe and orbitofrontal cortex due to the long TE needed for contrast to develop. In alt-SSFP images

(Fig 7, top), due to short TR/TE and banding suppression from phase cycling, the functional sensitivity and hence activation maps extend into and partially recover these signal dropout regions. The artifact-suppression and whole-brain imaging capability of alt-SSFP can be appreciated in Fig 8.

Fig 9 shows group analysis results from the visual stimulus experiment for GRE-EPI and alt-SSFP across N = 9 subjects, with maps thresholded identically. Alt-SSFP activation maps showed good agreement with GRE-EPI in terms of spatial extent. Alt-SSFP exhibits lower functional sensitivity compared to GRE-EPI, as expected, due to higher spatial specificity and reduced sources of contrast from larger veins. Nonetheless, alt-SSFP demonstrates good functional sensitivity to neuronal activation.

## Discussion

In this work we presented a fat-suppressed alt-SSFP method for fMRI and demonstrated good BOLD sensitivity through both breath-hold and visual stimulus functional experiments.

### BOLD Sensitivity

We have shown that alternating-SSFP maintains good BOLD sensitivity even with catalyzing transitions in and out of steady states. For our proposed alt-SSFP implementation with a flip angle of 35°, a TR = 14.3 ms was used. The flip angle was chosen to maintain sufficient contrast while minimizing the frequency sensitivity of the signal magnitude and phase over a range of off-resonance frequencies (14). MIP was used for image combination to avoid mixing of transition band and pass-band signal. BOLD contrast and functional sensitivity were reduced for alt-SSFP compared to conventional GRE EPI which is consistent with previous work (37), but visual stimulation maps from each protocol were spatially in agreement.

Applying the fat-suppression SPSP RF pulse in the context of bSSFP results in an erratic spectral profile outside of approximately ±200 Hz (Fig 3(b)). Regions of the brain such as the orbital frontal region that are difficult to shim may suffer from some loss of contrast. For example, in Fig 7, although much of the BOLD sensitivity in signal dropout regions are recovered compared to conventional GRE acquisitions, they are not completely recovered. Nevertheless, the available banding-artifact-free spectral range in fat-suppressed alt-SSFP is still much wider (±200 Hz) than what is available for conventional pb-SSFP (1/TR, or ±50 Hz for TR = 10 ms). Simulations of contrast vs. off-resonance profiles for alt-SSFP with and without the SPSP pulse (in Sup Fig S1, available online) demonstrated that despite the erratic spectral profile outside of ±200 Hz, normal pb-SSFP functional contrast still holds within this ±200 Hz banding-artifact-free range for fat-suppressed alt-SSFP.

In order to accommodate SPSP excitation pulses and EPI echo-time shifting, the TR used in our alt-SSFP implementation is longer than what is conventionally used in pb-SSFP fMRI studies (10). The slight increase in TR used in alt-SSFP compared to conventional lengths of less than 10 ms should result in increased signal change percentage (9,37). On the other hand, previous studies have shown that small-vessel specificity improves with increased TR

for values less than 16 ms before getting worse (11). Conventionally, longer TRs are not used so as to avoid having more banding artifacts in the FOV, but in alt-SSFP, banding artifacts are suppressed. Therefore, we expect better BOLD contrast using alt-SSFP than from previous pb-SSFP implementations, both from the increased TR values permitted, as well as the increased tSNR resulting from fat suppression.

### Fat Signal Suppression

Fat signal suppression is important for fMRI applications using bSSFP for several reasons. Fat signal is very bright in bSSFP acquisitions (high $T_2/T_1$ ratio), and fat signal that is displaced from the skull into the peripheral GM regions of the brain can cause Brain Extraction Tools (BET) to fail (as shown in Figure 5(a)). Errors in brain extraction reduce the accuracy of motion correction, intra-subject registration of low-resolution raw images and high-resolution anatomical scans, and the reliability of fMRI statistical analyses. In addition, fat signal is prone to unstable catalyzation since it is off-resonance from the water peak where catalyzation schemes are optimized (16).

In our results, we found increased tSNR when fat-suppression was applied. This could be because fat exhibits off-resonance instabilities which produce unstable EPI phase-encode ghosts throughout the brain, but is undetectable visually. Although using linear flip angle preparation reduces off-resonance signal oscillations compared to methods such as $\alpha/2$ catalyzation, signal oscillations due to off-resonance may still be an issue when relatively few catalyzation pulses are used (16). Off-resonance fat signal may experience irregular oscillatory patterns from TR to TR during RF catalyzation that results in ghosting that varies from volume to volume. We hypothesize that this is the cause of the global change in tSNR rather than a change localized to structured ghosting regions, and requires more investigation to verify. Although SPSP RF pulses are relatively long and result in some loss of efficiency in the sequence, with the added benefits of fat suppression and the capability of the proposed alt-SSFP sequence to accommodate for this relatively longer TR, the loss of efficiency does not appear to be detrimental. In our work we have demonstrated that including a short SPSP RF pulse not only suppresses bright fat signal that may confound brain segmentation and motion-correction analysis, but also increases tSNR overall, improving functional BOLD sensitivity.

Other forms of fat suppression have been employed in bSSFP sequences, including magnetization preparation techniques such as chemical saturation (38). However, the requirement that alt-SSFP image volumes encode the k-space center at then end of the acquisition train for optimal BOLD contrast causes these approaches to fail as suppressed fat signal regrows over this 1 – 2 s time frame.

There is a design tradeoff between the sharpness of the spatial profile and the width of the fat stop-band in the spectral profile of the SPSP RF pulse. For alt-SSFP, it is important to ensure uniform flip angle across the excited slab due to the sensitivity of the SSFP off-resonance profile to flip angle (21). Therefore, a sharp spatial profile was prioritized by implementing minimum-phase sub-pulses. We found that the fat null $\Delta B_0$ tolerance to be sufficient for robust fat suppression in all subjects. However, other tradeoffs are possible for different requirements and design choices.

### Temporal Resolution

Our alt-SSFP sequence has a volume time of 3.46 s, which is relatively long for standard fMRI sequences. Therefore, it is important that additional acceleration is included for future implementations to achieve a total volume time under 3 s. For example, acceleration could be implemented in two directions, $k_y$ and $k_z$, which would accommodate higher acceleration factors in accordance to coil geometries. Methods such as compressed sensing could also be explored. Higher acceleration would allow higher resolution whole-brain coverage with voxel sizes of ≤ 3 mm. This would be beneficial, as residual signal dropout artifacts in fat-suppressed alt-SSFP (Fig 7) may be due to the relatively large slice thickness of 5 mm used in the breath-hold experiments. Prescribing higher-resolution scans would reduce susceptibility effects. On the other hand, faster acquisitions and shorter volume times may allow for more phase-cycling steady-states (instead of just two) to alternate between, which would potentially increase the signal and contrast uniformity of the MIP results. Ultimately, the temporal resolution of alternating SSFP is limited by the time required to establish a stable signal and recover BOLD contrast following a change in the RF phase cycling increment (14).

### Respiration-induced Frequency Shift

Respiration-induced frequency shift correlated with the functional paradigm was a particular complication for breath-hold fMRI data analyses for our study. $B_0$ fluctuations induced by susceptibility changes during respiration cause resonance offsets in the brain. These $B_0$ fluctuations are caused by varying lung volume and movements in the chest and diaphragm (39,40). In the pass-band region of the SSFP off-resonance profile, these resonance offsets have little effect. However, near the transition-band regions, respiration-induced frequency shift produces respiration-correlated signal intensity changes that results in artificially high functional activation that is not caused by BOLD contrast. For analysis of individual phase-cycling image time courses (phase-cycling 0° or phase-cycling 180°), these high activation scores near transition-band are apparent (Fig 4). In general, MIP reconstruction suppresses the respiration-induced frequency-shift activation artifact naturally by not selecting image phases from these afflicted regions based on the average raw functional image of the scan. However, there can still exist a small overlap transition-band region between the two phase-cycling off-resonance diagrams that is sometimes sensitive to this behavior. It is important to remember that this is a unique challenge in breath-hold paradigms using bSSFP acquisitions and is not expected to a ect most other fMRI paradigms where breathing is not strongly correlated with functional paradigm. Some methods to directly mitigate these artifacts include real-time frequency-shift compensation (39) or directly performing hypercapnia experiments by delivering different fractions of $CO_2$, $O_2$ and $N_2$ gas mixtures to subjects periodically instead of voluntary breath holding (41).

### Maximum Intensity Projection

In these studies a MIP mask was computed from the average raw image over the entire time course. This is based on the underlying assumption that a voxel has higher signal in the same phase-cycling steady-state throughout the entire time course. However, to a certain degree during all studies, banding artifacts have the potential to spatially shift throughout the fMRI

time-course due to respiratory-induced field changes, or resonance frequency drift originating from system factors such as the gradient systems. Currently, online band drift correction is not employed. A different method for MIP would be to compute pair-wise MIP masks for each phase-cycled volume pair. Using pairwise MIP masks could potentially better track the drifting of bSSFP bands throughout the entire time course to result in more accurate alignment. In this work involving block paradigms, band drifting did not appear to be problematic; we found both of these MIP methods to give similar results, as shown in Fig 4.

It is important to note that certain fMRI processing steps require some care when applying the MIP operation, using either mean image based MIPs or MIPs done individually with each volume pair. In event-related fMRI, it is especially important to know the precise timing of each acquisition volume relative to each stimuli event. Therefore, it would be essential to keep track of which phase-cycling volume a voxel came from, since the two volumes would correspond to different acquisition times (separated by half the total volume acquisition time). Fundamentally this information is available and could be incorporated into event-related design processing stages. Similar considerations would be needed for any temporal filtering applied, with the precise acquisition time for each voxel in the time course, based on the index selected by the MIP, being required for ideal filter application. Also, processing steps like RETROICOR (42), which takes physiological noise into account, would need to be done prior to MIP reconstruction since the two phase-cycled steady-states occur during different parts of the cardiac and respiratory cycles.

### GRAPPA Auto-calibration

Although band drifting was not observed to be problematic for the paradigms used in our study, it may be important to implement an auto-calibrated EPI trajectory for some studies where motion correction or coil-unwrap aliasing artifacts are present. Currently, a fully-encoded volume is acquired at the beginning of the fMRI scan from which GRAPPA weights are derived for reconstruction of the entire scan. Ideally, GRAPPA weights should be computed on a volume-by-volume basis. By including an autocalibration region in every single volume to compute GRAPPA weights for each time point rather than using the same weights throughout, alt-SSFP should be able to track each volume and the possible shifting of banding artifacts more accurately through time. Motion correction algorithms prior to data analysis would therefore be able to more accurately align the temporal volumes as well. The competing issue would be the increased time required to collect the auto-calibration phase encode data that would result in increased image volume TR or reduced slice spatial coverage.

## Conclusion

We have developed a practical balanced-SSFP fMRI method that permits whole-brain coverage in a single fMRI scan with good BOLD sensitivity. We have made alt-SSFP applicable for human fMRI studies by incorporating flyback-EPI, echo-time shifting, parallel imaging, and fat suppression. Through breath-holding and visual stimulus paradigm

experiments, we have demonstrated the capability of alt-SSFP to perform functional imaging in regions that are currently inaccessible to conventional pb-SSFP and GRE methods.

## Supplementary Material

Refer to Web version on PubMed Central for supplementary material.

## Acknowledgements

The authors would like to thank Atsushi Takahashi, Bob Dougherty, and Adam Kerr for their help. This material is based upon work supported by the National Institutes of Health under award number R01EB006471 and the National Science Foundation Graduate Research Fellowship Program under grant number DGE-1147470.

## References

1. Ogawa S, Tank DW, Menon R, Ellermann JM, Kim SG, Merkle H, Ugurbil K. Intrinsic signal changes accompanying sensory stimulation: functional brain mapping with magnetic resonance imaging. Proceedings of the National Academy of Sciences of the United States of America. 1992; 89:5951–5. [PubMed: 1631079]
2. Bandettini PA, Wong EC, Jesmanowicz A, Hinkst RS, Hyde JS. Spin-Echo and Gradient-Echo EPI of Human Brain Activation using BOLD Contrast : a Comparative Study at 1.5 T. NMR Biomed. 1994; 7:12–20. [PubMed: 8068520]
3. Norris DG. Spin-echo fMRI: The poor relation? NeuroImage. 2012; 62:1109–15. [PubMed: 22245351]
4. Sun H, Fessler Ja, Noll DC, Nielsen JF. Steady-state functional MRI using spoiled small-tip fast recovery imaging. Magn Reson Med. 2014; 00:1–8.
5. Scheffler K, Seifritz E, Bilecen D, Venkatesan R, Hennig J, Deimling M, Haacke ME. Detection of BOLD changes by means of a frequency- sensitive trueFISP technique : preliminary results. NMR Biomed. 2001:490–496. [PubMed: 11746942]
6. Miller KL, Hargreaves Ba, Lee J, Ress D, DeCharms RC, Pauly JM. Functional brain imaging using a blood oxygenation sensitive steady state. Magn Reson Med. 2003; 50:675–83. [PubMed: 14523951]
7. Miller KL, Smith SM, Jezzard P, Pauly JM. High-resolution FMRI at 1.5T using balanced SSFP. Magn Reson Med. 2006; 55:161–70. [PubMed: 16345040]
8. Bowen, CV.; Menon, RS.; Gati, JS. Proceedings of the 13th Annual Meeting of ISMRM. Miami: 2005. High field balanced-SSFP fMRI : A BOLD technique with excellent tissue sensitivity and superior large vessel suppression.; p. 119
9. Miller KL, Smith SM, Jezzard P, Wiggins GC, Wiggins CJ. Signal and noise characteristics of SSFP FMRI: a comparison with GRE at multiple field strengths. NeuroImage. 2007; 37:1227–36. [PubMed: 17706432]
10. Lee JH, Dumoulin SO, Saritas EU, Glover GH, Wandell Ba, Nishimura DG, Pauly JM. Full-brain coverage and high-resolution imaging capabilities of passband b-SSFP fMRI at 3T. Magn Reson Med. 2008; 59:1099–110. [PubMed: 18421687]
11. Kim TS, Lee J, Lee JH, Glover GH, Pauly JM. Analysis of the BOLD Characteristics in Pass-Band bSSFP fMRI. Int J Imaging Syst Technol. 2013; 22:23–32. [PubMed: 23661904]
12. Dharmakumar R, Qi X, Hong J, Wright GA. Detecting microcirculatory changes in blood oxygen state with steady-state free precession imaging. Magn Reson Med. 2006; 55:1372–80. [PubMed: 16680697]
13. Miller KL, Jezzard P. Modeling SSFP functional MRI contrast in the brain. Magn Reson Med. 2008; 60:661–73. [PubMed: 18727099]
14. Patterson, S. PhD thesis. Dalhousie University; 2013. “Alternating SSFP Permits Rapid, Banding-Artifact-Free Balanced SSFP fMRI”..

15. Scheffler K, Lehnhardt S. Principles and applications of balanced SSFP techniques. Eur Radiol. 2003; 13:2409–18. [PubMed: 12928954]
16. Deshpande VS, Chung YC, Zhang Q, Shea SM, Li D. Reduction of transient signal oscillations in true-FISP using a linear flip angle series magnetization preparation. Magn Reson Med. 2003; 49:151–7. [PubMed: 12509831]
17. Meyer CH, Pauly JM, Macovski A, Nishimura DG. Simultaneous spatial and spectral selective excitation. Magn Reson Med. 1990; 15:287–304. [PubMed: 2392053]
18. Block W, Pauly JM, Kerr A, Nishimura DG. Consistent fat suppression with compensated spectral-spatial pulses. Magn Reson Med. 1997; 38:198–206. [PubMed: 9256098]
19. Zur Y. Design of Improved Spectral-Spatial Pulses for Routine Clinical Use. Magn Reson Med. 2000; 43:410–420. [PubMed: 10725884]
20. Yuan J, Madore B, Panych LP. Fat-water selective excitation in balanced steady-state free precession using short spatial-spectral RF pulses. J Magn Reson. 2011; 208:219–24. [PubMed: 21134770]
21. Carr H. Steady-State Free Precession in Nuclear Magnetic Resonance. Phys Rev. 1958:1693–1701.
22. John, TS. PhD thesis. Stanford University; 2011. “Advances and Improvements in Three-Dimensional Functional Magnetic Resonance Imaging”..
23. Feinberg DA, Oshio K. Phase errors in multi-shot echo planar imaging. Magn Reson Med. 1994; 32:535–539. [PubMed: 7997122]
24. Butts K, Riederer SJ, Ehman RL, Thompson RM, Jack CR. Interleaved echo planar imaging on a standard MRI system. Magn Reson Med. 1994; 31:67–72. [PubMed: 8121272]
25. Hargreaves, Ba; Vasanawala, SS.; Pauly, JM.; Nishimura, DG. Characterization and reduction of the transient response in steady-state MR imaging. Magn Reson Med. 2001; 46:149–58. [PubMed: 11443721]
26. Deimling, M.; Heid, O. Magnetization prepared trueFISP imaging.. Proceedings of the 2nd Annual Meeting of ISMRM; San Francisco. 1994; p. 495
27. Nishimura, DG.; Vasanawala, S. Analysis and Reduction of the Transient Response in SSFP Imaging.. Proceedings of the 8th Annual Meeting ISMRM; Denver. 2000; p. 301
28. Le Roux P. Simplified model and stabilization of SSFP sequences. J Magn Reson. 2003; 163:23–37. [PubMed: 12852904]
29. Pauly JM, Roux PL, Nishimura DG, Macovski A. Parameter relations for the Shinnar-Le Roux selective excitation pulse design algorithm. IEEE Trans Med Imag. 1991
30. Griswold, Ma; Jakob, PM.; Heidemann, RM.; Nittka, M.; Jellus, V.; Wang, J.; Kiefer, B.; Haase, A. Generalized autocalibrating partially parallel acquisitions (GRAPPA). Magn Reson Med. 2002; 47:1202–10. [PubMed: 12111967]
31. Kastrup, a; Li, TQ.; Takahashi, a; Glover, GH.; Moseley, ME. Functional Magnetic Resonance Imaging of Regional Cerebral Blood Oxygenation Changes During Breath Holding. Stroke. 1998; 29:2641–2645. [PubMed: 9836778]
32. Peirce JW. Generating Stimuli for Neuroscience Using PsychoPy. Frontiers in Neuroinformatics. 2009; 2:1–8.
33. Smith SM, Jenkinson M, et al Woolrich MW. Advances in functional and structural MR image analysis and implementation as FSL. NeuroImage. 2004; 23(Suppl 1):S208–19. [PubMed: 15501092]
34. Jenkinson M, Bannister P, Brady M, Smith S. Improved Optimization for the Robust and Accurate Linear Registration and Motion Correction of Brain Images. NeuroImage. 2002; 17:825–841. [PubMed: 12377157]
35. Zhang Y, Brady M, Smith S. Segmentation of brain MR images through a hidden Markov random field model and the expectation-maximization algorithm. IEEE Trans Med Imag. 2001; 20:45–57.
36. Eickhoff SB, Stephan KE, Mohlberg H, Grefkes C, Fink GR, Amunts K, Zilles K. A new SPM toolbox for combining probabilistic cytoarchitectonic maps and functional imaging data. NeuroImage. 2005; 25:1325–35. [PubMed: 15850749]

37. Zhong K, Leupold J, Hennig J, Speck O. Systematic investigation of balanced steady-state free precession for functional MRI in the human visual cortex at 3 Tesla. Magn Reson Med. 2007; 57:67–73. [PubMed: 17191247]

38. Scheffler K, Heid O. Magnetization Preparation During the Steady State : Fat-Saturated 3D TrueFISP. Magn Reson Med. 2001; 45:1075–1080. [PubMed: 11378886]

39. Lee J, Santos JM, Conolly SM, Miller KL, Hargreaves Ba, Pauly JM. Respiration-induced B0 field fluctuation compensation in balanced SSFP: real-time approach for transition-band SSFP fMRI. Magn Reson Med. 2006; 55:1197–201. [PubMed: 16598728]

40. Van de Moortele PF, Pfeuffer J, Glover GH, Ugurbil K, Hu X. Respiration-induced B0 fluctuations and their spatial distribution in the human brain at 7 Tesla. Magn Reson Med. 2002; 47:888–95. [PubMed: 11979567]

41. Rostrup E, Larsson HB, Toft PB, Garde K, Thomsen C, Ring P, Sondergaard L, Henriksen O. Functional MRI of CO2 induced increase in cerebral perfusion. NMR Biomed. 1994; 7:29–34. [PubMed: 8068522]

42. Glover GH, Li TQ, Ress D. Image-Based Method for Retrospective Correction of Physiological Motion Effects in fMRI: RETROICOR. Magn Reson Med. 2000; 44:162–167. [PubMed: 10893535]

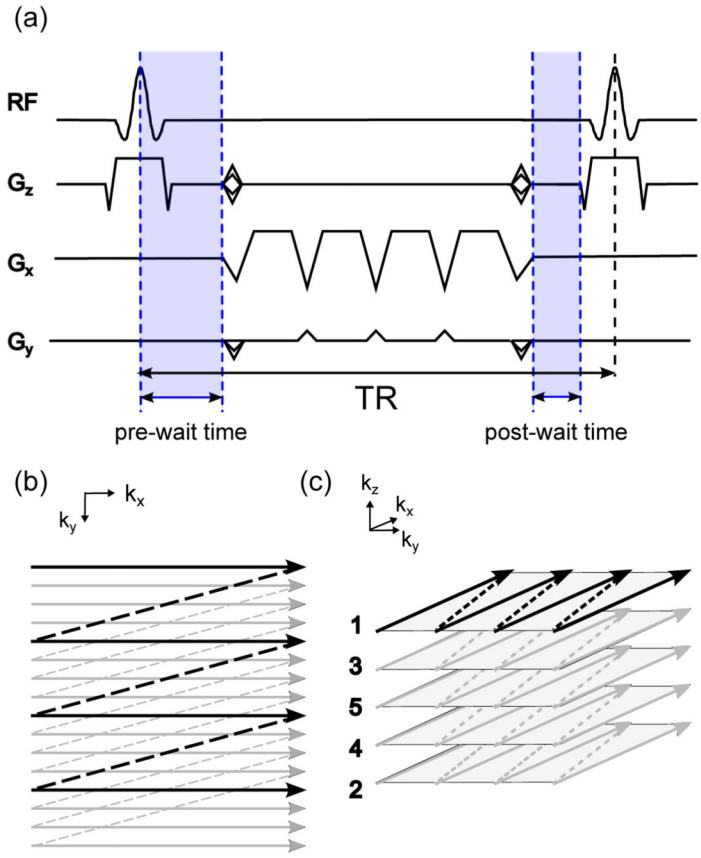


**FIG. 1.**

**a:** Pulse sequence diagram for multi-shot flyback-EPI bSSFP fMRI with an echo-train length of 4. At each excitation, echo-time shifting is carried out by delaying the data acquisition train by adding a Δt to the initial pre-wait time and reducing the initial post-wait time by the same amount for the next shot. Therefore, the abrupt changes in phase are smoothed out and the ghosting is reduced greatly. **b:** In-plane $k_x$-$k_y$ flyback-EPI trajectory. **c:** 3D k-space traversal order: numbers correspond to order of acquisition. k-Space z-encodes are in reverse-centric order to acquire the center of k-space near the end of the volume time.

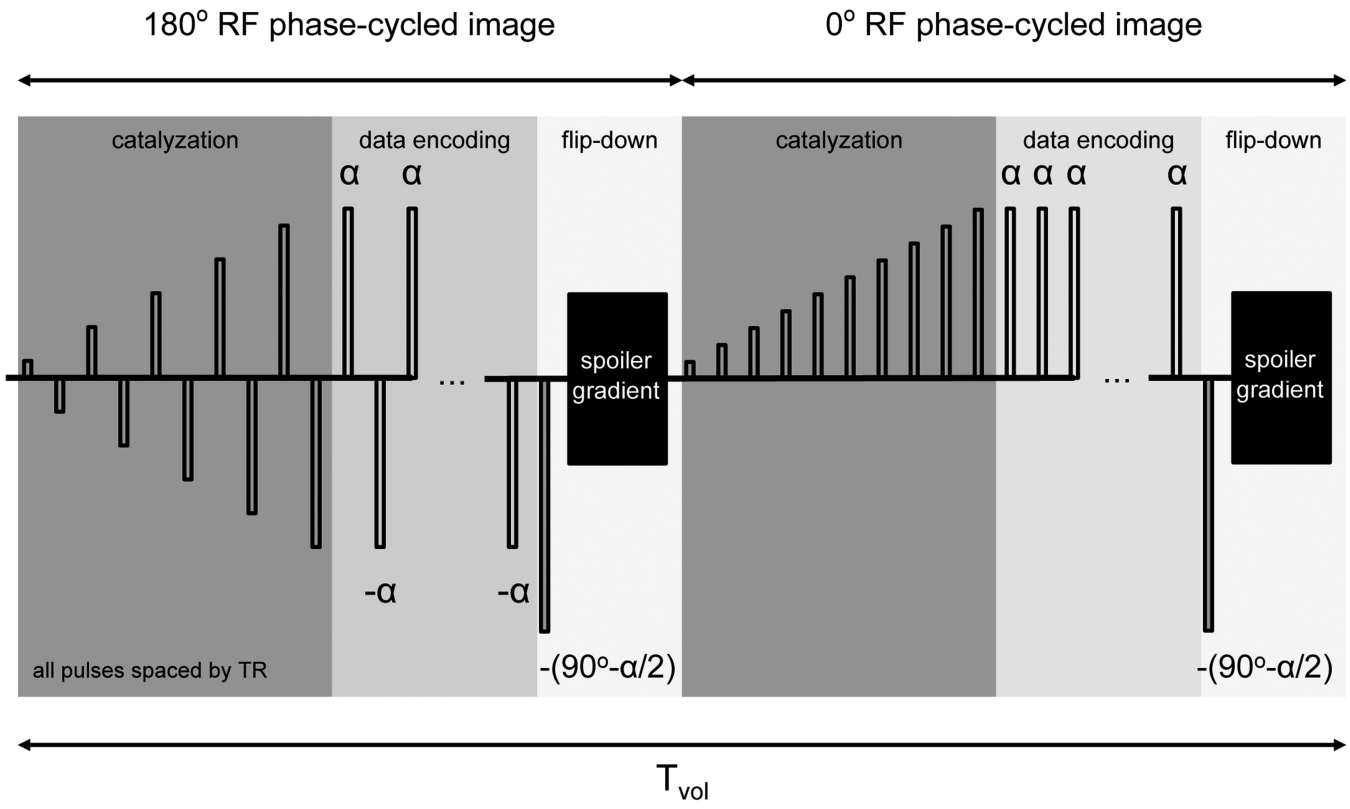


**FIG. 2.**

Alternating-SSFP (alt-SSFP) catalyzation scheme. Alt-SSFP consists of continuously alternating between two phase-cycled steady states, 180° and 0°, throughout one fMRI scan. For each steady state, a complete 3D volume is acquired. Ten dummy cycles are used for RF linear flip-angle catalyzation at the beginning of each acquisition volume. At the end of each phase-cycled 3D acquisition volume, a 90°−$\alpha$/2 flip-down pulse after a full TR wait is applied, followed by gradient spoiling. Volume time $T_{vol}$ is defined as the total time to acquire a 180°, 0° phase-cycled image volume pair.

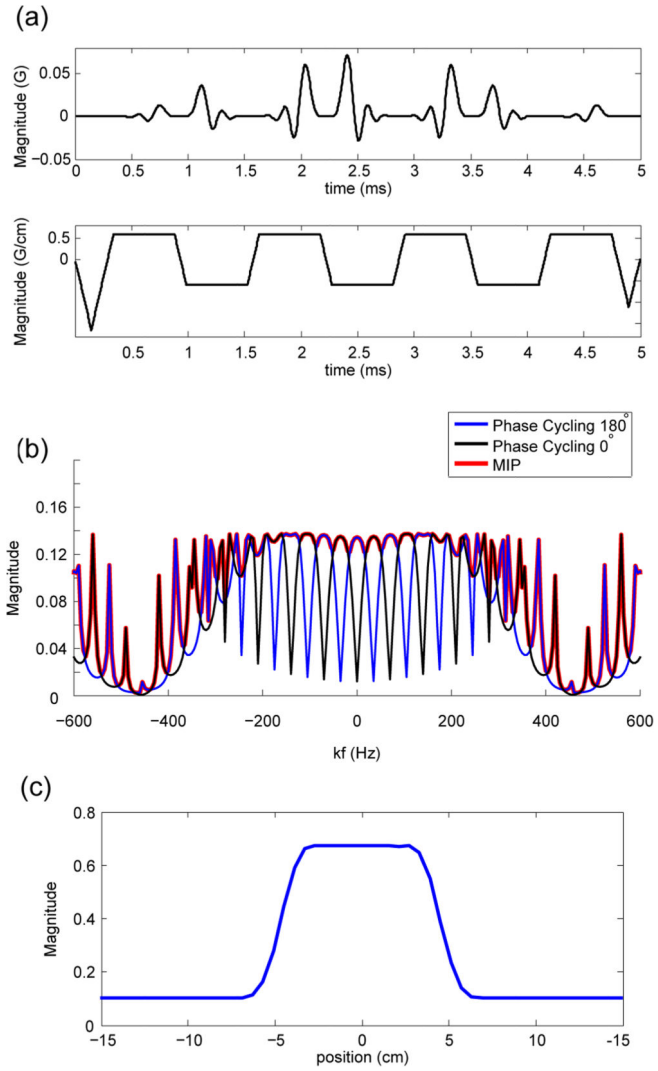


**FIG. 3.**

Short spatial-spectral (SPSP) RF pulse for fat-suppression. **a:** Spatial-spectral RF pulse and gradient waveforms. RF pulse was designed with 4.35 ms nominal duration resulting in a 5 ms RF excitation for each TR. **b:** Steady-state spectral profile simulation of the SPSP RF pulse. The blue line represents the spectral profile of the 180° phase-cycled steady state, and the black line represents the spectral profile of 0° phase-cycled steady state. MIP profile (red) is fairly uniform near the on-resonance region, while a spectral null was designed at −440 Hz (fat chemical shift at 3T). **c:** Spatial profile of SPSP RF pulse for a slab width of 9.9cm.

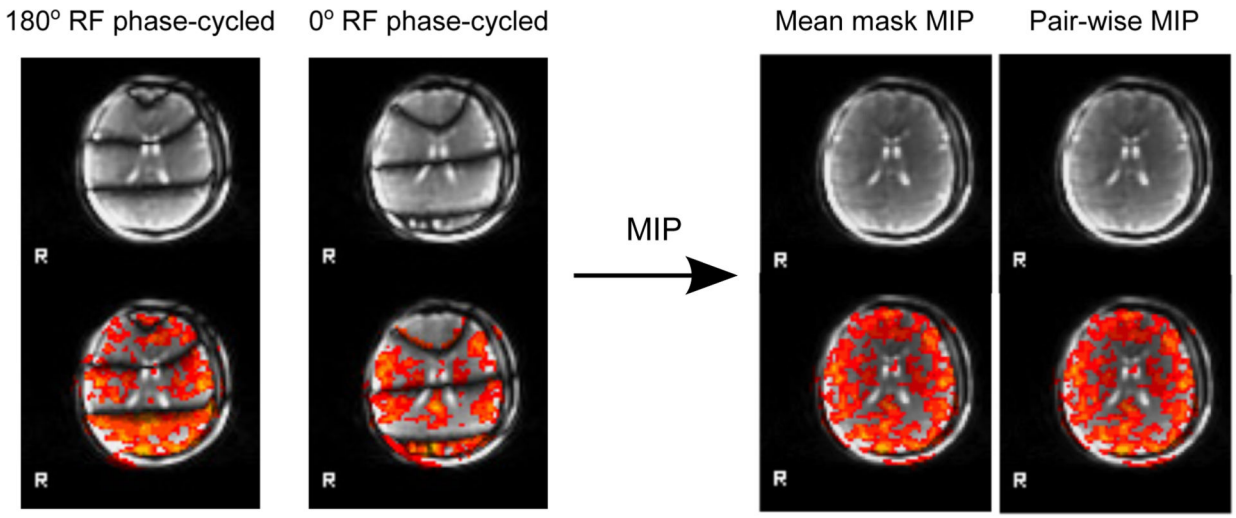


**FIG. 4.**

Banding artifact reduction by alt-SSFP in a single fMRI scan. Images from a representative subject show both 180° RF phase-cycled and 0° RF phase-cycled images exhibit low signal stop-bands with no functional activation. Two possible Maximum Intensity Projection (MIP) methods were considered: 1) computing one mask based on the mean signal intensity over the entire time-course, and 2) computing a mask for every image volume pair. The first method was chosen for this study to be consistent with two-acquisition pb-SSFP fMRI (10). Our results showed minimal difference between the two methods. MIP combination of the phase-cycled image volume pairs recovers stop band signal and results in relatively uniform functional sensitivity. Notice the bright fat-shift artifact that exists prior to applying fat-suppression.

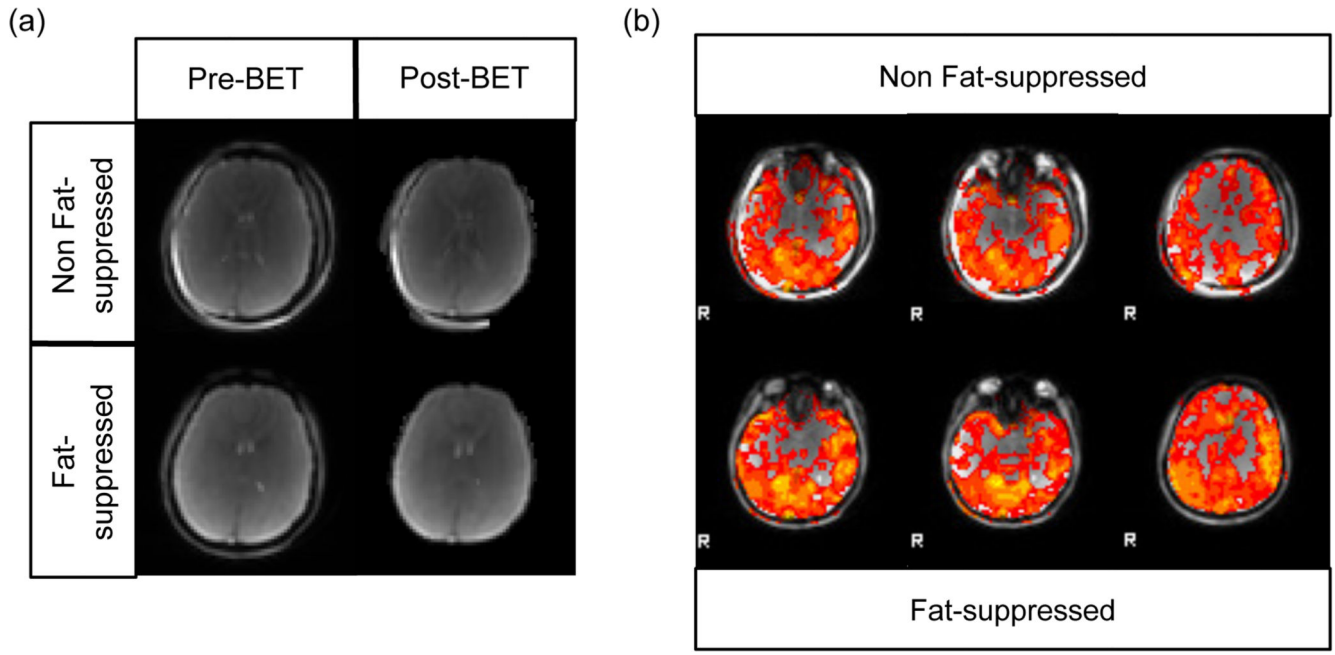


**FIG. 5.**

**a:** Before and after applying the Brain Extraction Tool (BET) in FSL. The coherent fat shift into the brain causes errors in brain extraction prior to intra-subject registration which may propagate through fMRI data analysis. **b:** Select slices from a breath-holding study of a representative subject, comparing non fat-suppressed alt-SSFP vs. fat-suppressed alt-SSFP results. By including the fat suppression spatial-spectral RF pulse, the bright fat signal shift (present in the top row) was greatly reduced. Fat-suppression results exhibit improved activation maps regarding z-scores and coverage.

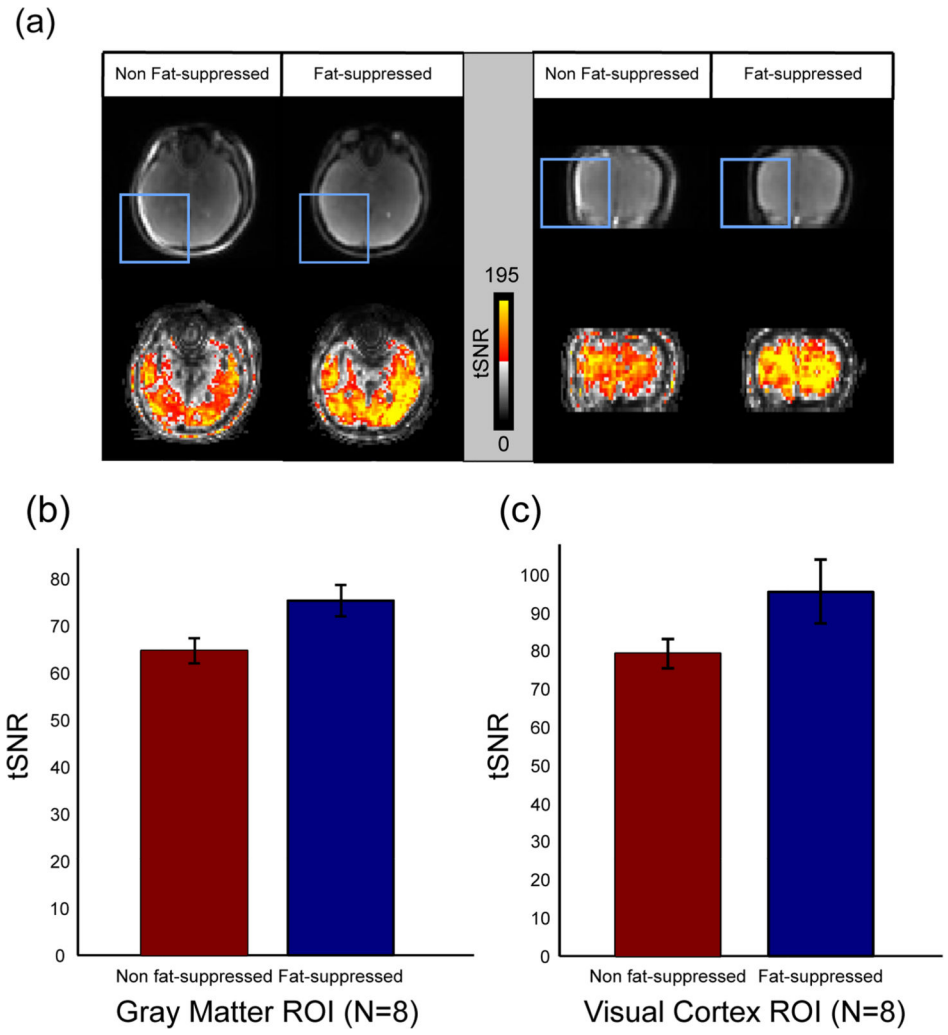


**FIG. 6.**

Observed temporal SNR (tSNR) increase in fat-suppressed alt-SSFP results compared to non fat-suppressed results. **a:** Select slices from a breath-holding study of a representative subject. Raw images (top) show bright fat signal shift into the brain volume (in boxes) without fat suppression (left: axial, right: coronal). By using the designed short SPSP pulse, the bright fat signal is well suppressed. tSNR maps show that applying fat suppression increases temporal stability in fat-shift artifact regions and overall. **b:** The mean tSNR was calculated for all subjects over gray matter mask ROI over N = 8 subjects. Fat-suppressed results have an increase of 17% ± 4% mean tSNR over non fat-suppressed results. **c:** Mean tSNR was computed within the V1 region of the visual cortex over N = 8 subjects. Fat-suppressed results have an increase of 20% ± 8% over non fat-suppressed results.

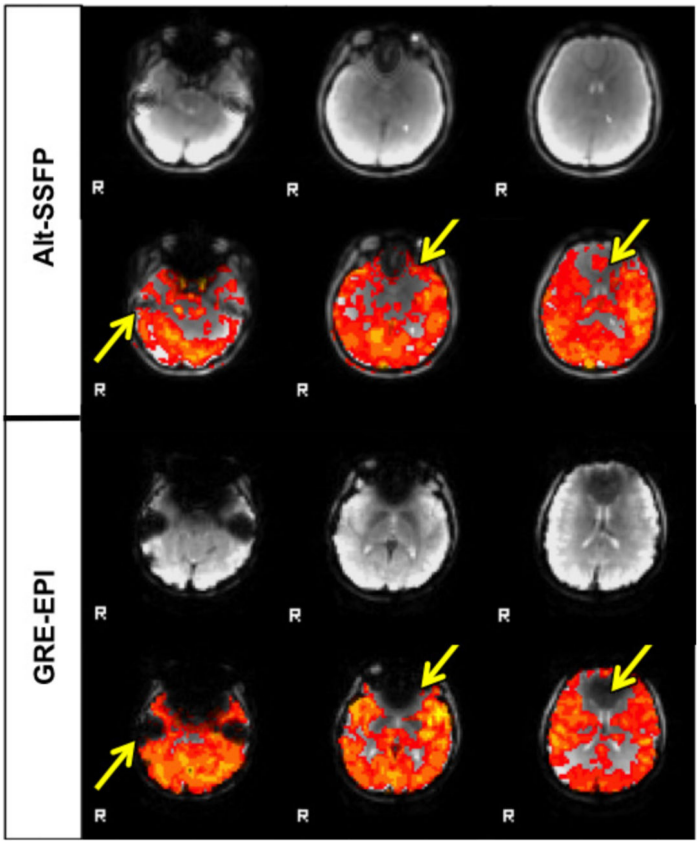


**FIG. 7.**

Select slices from a breath-holding study of a representative subject. Areas such as temporal lobe and orbitofrontal cortex regions suffer from signal dropout in GRE-EPI due to severe magnetic field distortions around air-tissue interfaces. In fat-suppressed alt-SSFP, both raw signal magnitude and functional sensitivity of these regions are greatly recovered.

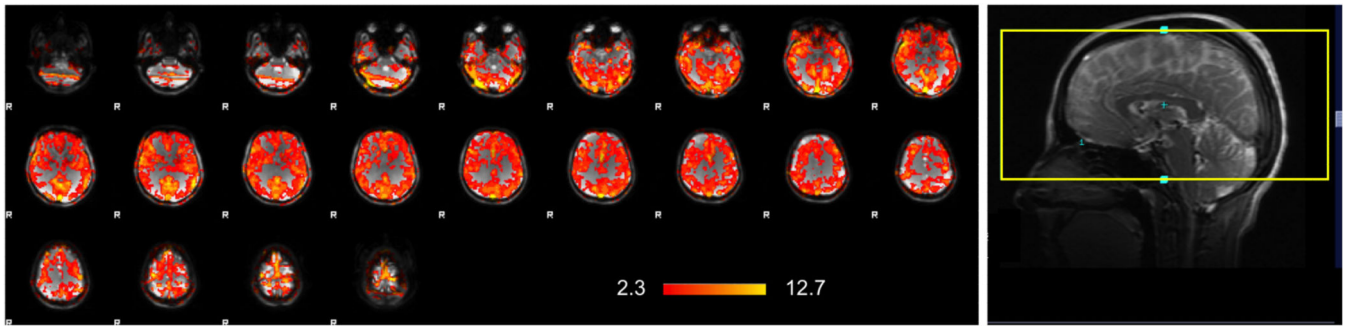


**FIG. 8.**

Example of whole brain alt-SSFP activation map from a breath-holding study of a representative subject. Banding artifacts from conventional b-SSFP acquisitions and signal dropout from conventional GRE-EPI are greatly recovered, resulting in relatively uniform activation maps. The scan prescription screenshot on the right demonstrates the volumetric coverage extent which covers the entire brain. A few end slices suffering from lower flip-angle (due to the transition band of the RF pulse spatial profile) result in high activation adjacent to the bands and may be thrown out as in other sequences and still retain a wide coverage.

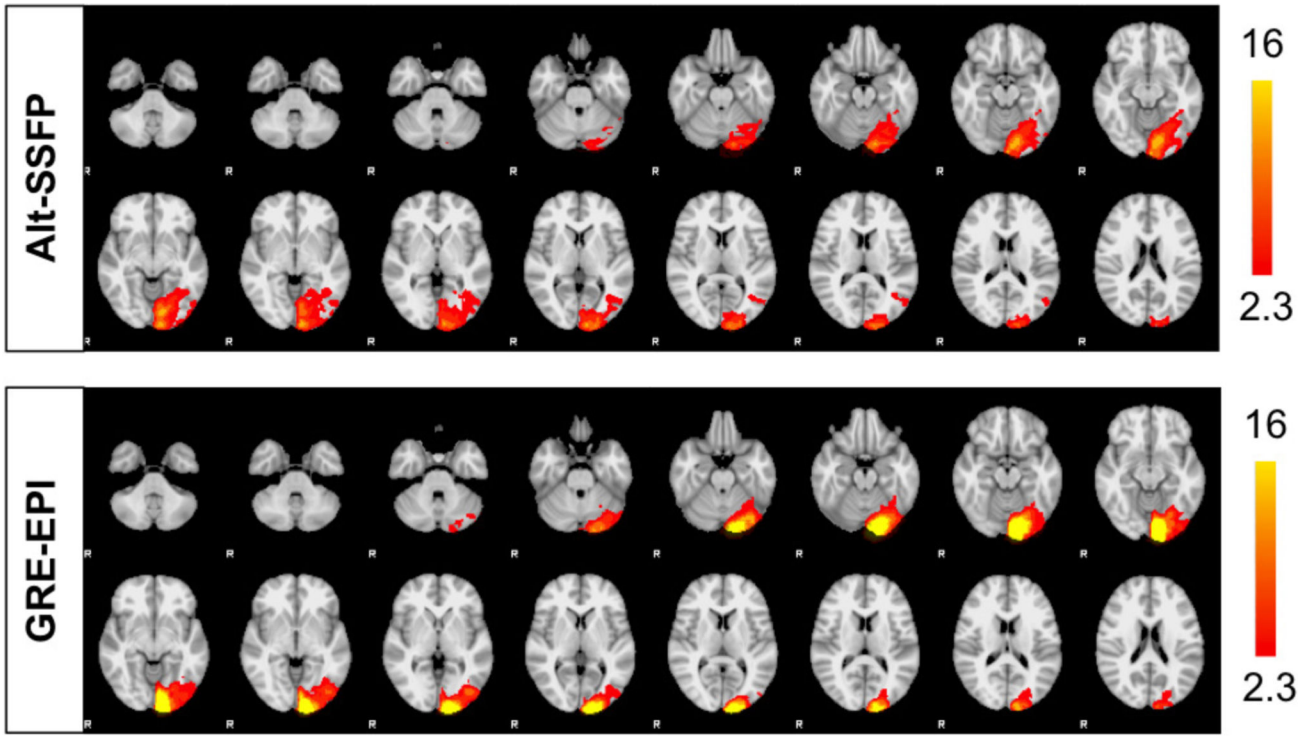


**FIG. 9.**

Comparison of group statistics of visual stimulus study between GRE-EPI and fat-suppressed alt-SSFP, overlaid on a standard brain. Fixed effect group analysis was used to analyze mean activation over N = 9 subjects. Fat-suppressed alt-SSFP show good agreement with spatial extent of GRE-EPI activation results and exhibit good sensitivity to neuronal activation.